



# Optimal Layout Method of Multiple Vibration Sensors Based on Motor Vibration Frequency Response

Feng Zhou<sup>1</sup> · Pengcheng Xu<sup>1</sup> · Xingzhen Bai<sup>1</sup> · Hao Wang<sup>1</sup> · Huakun Bi<sup>1</sup> · Baochun Cui<sup>1</sup>

Received: 23 November 2021 / Revised: 9 June 2022 / Accepted: 14 June 2022 / Published online: 2 July 2022  
© Krishtel eMaging Solutions Private Limited 2022

## Abstract

**Purpose** The optimal measurement points for the vibration characteristics of the motor under different faults may be inconsistent, which results in the problem that the motor cannot obtain reliable vibration signals during fault diagnosis or condition monitoring. However, the existing research seldom considers the influence of the installation position of the vibration sensor on the diagnosis effect. Therefore, this paper proposes an optimal layout method for vibration sensors based on the frequency response of motor vibration.

**Methods** This paper analyzes the air gap magnetic field of the motor and obtains the changes of the radial electromagnetic force wave of the motor under normal operation, eccentric operation and broken rotor bars operation. Electromagnetic excitation is applied to the motor model and different base constraints are set to obtain the three-dimensional vibration characteristics of the shell under normal operation, eccentric operation and broken rotor bars operation. According to the vibration characteristics of the shell, the vibration laws under different working conditions are obtained. According to the three-dimensional vibration characteristics of the motor, the optimal vibration measurement points are selected and a new type of vibration sensors layout scheme is designed.

**Conclusion** The results showed that the motor has different vibration optimal measuring points under different operating states. In addition, the identification and diagnosis of motor faults can be realized through the joint analysis of multiple vibration sensors after the optimized layout.

**Keywords** Frequency response · Motor vibration · Motor eccentricity · Motor broken bar · Optimal measuring point · Sensor layout

## Introduction

With the improvement of the industrialization level, the application of motors has become more and more extensive. It is becoming more and more important to carry out accurate and effective condition monitoring and fault diagnosis of the motor. Every year around the world, a large number of economic losses and safety accidents are caused by motor failures [1]. Most of the motor faults are always accompanied by abnormal motor vibration, which means that monitoring the vibration signals of the motor can effectively identify a variety of motor faults, and it has always

been a research hotspot in the field of motor monitoring and fault diagnosis. Cruz-Vega et al. designed a new type of broken bar automatic detection algorithm based on the vibration signals of the motor, which can detect the damage before the rotor bar is broken [2]. Morales-Perez et al. proposed an Orthogonal Matching (OMP) algorithm based on the motor vibration signals, which can accurately diagnose the extremely small rotor bar cracks [3]. EKER proposed an Angular Domain-Order Tracking method based on motor vibration signals to diagnose motor eccentricity faults [4]. Panigrahy uses the three-dimensional vibration signals to diagnose the fault of the motor and it has shown that the three-dimensional vibration signals can reflect the deeper vibration characteristics of the motor [5].

Many motor diagnosis algorithms are based on accurate vibration signals. The data accuracy of motor vibration signals will directly affect the results of the motor diagnosis, and even lead to false alarms or untimely alarms. The

✉ Feng Zhou  
f.zhou@163.com

<sup>1</sup> College of Electrical Engineering and Automation, Shandong University of Science and Technology, Qingdao 266590, Shandong, China

installation position of the vibration sensors directly determines the accuracy of the vibration characteristics collected by the vibration sensors, and it is a vital part in the field of motor monitoring. Xin has analyzed the differences in the data collected by the piezoelectric acceleration sensor in the adhesive bonding and magnetic base installation methods and proved that different installation methods will affect the data collected by the sensor [6]. Xunwen et al. has proposed a vibration sensor optimization layout method based on the sensitivity of the fault frequency, and determined the best installation position of the vibration sensor of the reducer at the end face of the bearing seat [7]. In view of the phenomenon of frequent over-vibration triggering protection actions of wind turbines, Tianling and Weiqiu studied the anti-interference of the vibration sensor installation position and found that the vibration measurement is more accurate and reliable when the wind turbine vibration sensor is installed in the center of the tower [8]. Aiming at the phenomenon that the gearbox of wind turbines is prone to failure, Guilan et al. used structural analysis to find out the location of the vibration sensor corresponding to all the possible failures of the gearbox [9]. To find the best installation position of the vibration sensor, Bouzaouit regularly selected 9 measuring points on the drive motor of the fan unit, with each measuring point separated by  $22.5^\circ$  [10]. To overcome the unreliability of the data collected by the vibration sensor, some scholars use other methods to replace the vibration sensor for data acquisition. Huang and Yang uses current and position signals to estimate vibration harmonics and identify the vibration frequency from the estimated harmonics [11]. Dutta et al. uses an antenna instead of a sensor to obtain the vibration signals when the induction motor fails [12]. Roy et al. designed a non-contact vibration measurement system that can accurately identify the precise location of vibration through microwave radar and optical strobe [13]. Some scholars also used the method of changing the type of vibration sensor to solve the problem of unreliable data. For example, to solve the disadvantages of traditional vibration sensors such as high false alarm rate and susceptibility to electromagnetic interference, Zhang et al. uses FBG vibration sensors for motor vibration monitoring [14]. Li et al. developed a vibration sensor with nanometer resolution to improve the accuracy and reliability of vibration measurement [15]. Debnath et al. designed a new type of piezoelectric vibration sensor that can detect bearings or be used as a power source for fault monitoring systems [16].

The layout optimization of vibration sensors has been studied by scholars, but there are still some limitations. For example, only a single vibration condition of the monitoring equipment is analyzed, and the optimal installation position of the vibration sensor under different vibration conditions may not be the same. Most of the existing researches focus on special motors, and there is a lack of research on the

layout optimization of vibration sensors when monitoring common vibrations in General Motors. The accuracy of the vibration signals obtained by the sensorless method is not high, and the cost of the new technology vibration sensor is too high.

It can be seen from the foregoing, the current motor vibration monitoring rarely considers the influence of the sensor installation position on the acquisition of signals and diagnosis, and the motor may have different optimal measurement points under different operating states. The vibration signals of the motor measured at the optimal measuring point can better reflect the vibration characteristics of the motor in different operating states, and the joint analysis of vibration signals from multiple measuring points may better distinguish the characteristics of different faults, so as to more accurately judge the operating state of the motor and carry out fault identification and diagnosis.

There are many factors that cause abnormal vibration of the motor. The most common causes of abnormal vibration include fault types such as motor eccentricity, broken rotor bars, and inter-turn short circuits, as well as shafting faults such as bearing oil shortage and bearing cracks. Among them, the inter-turn short circuit is an electrical fault, and the diagnosis effect is better when the voltage and current signals are used. The shaft fault has an exclusive diagnosis system, and temperature diagnosis is often used. However, there is a lack of suitable diagnostic methods for motor eccentricity and broken rotor bars. Since these two kinds of faults will generate unbalanced magnetic tension, which will cause electromagnetic vibration, it is more accurate and convenient to use the vibration signals as the fault feature for diagnosis after the optimal layout of multiple sensors.

This paper calculates the radial electromagnetic force of a three-phase induction motor under normal operation, eccentric operation and broken rotor bars operation. Combining with the base constraint and electromagnetic excitation, the frequency response analysis of the motor is performed to obtain the vibration characteristics of the shell under different operating conditions. Based on this, a new set of installation layout schemes of motor vibration sensors are designed. This method can accurately obtain the three-dimensional vibration characteristics of the three-phase induction motor under different operating conditions, which provide reliable data support for the state monitoring of the motor, and also provide a reference solution for the installation of other types of motor vibration sensors.

This method provides a vibration sensors layout and installation scheme for studying the vibration diagnosis method of motor eccentricity fault, broken bar fault and loose base, which can collect more accurate motor vibration signals and provide more reliable data guarantee for the diagnosis algorithm. After the sensors layout is carried out in this method, fault identification and diagnosis can also be

carried out through the vibration acceleration measured by each sensor. The method in this paper is suitable for providing a new method and theoretical basis for the online vibration monitoring, fault diagnosis and life assessment of the motor in various manufacturing industries.

### Analysis of Radial Electromagnetic Force of Induction Motor

Frequency response analysis is to apply a series of periodic sinusoidal excitations of different frequencies to the system and analyze its steady-state response under the periodic excitation. The main excitation source of three-phase induction motor vibration is the radial electromagnetic force on the inner wall of the stator [17].

The harmonics in the air gap of asynchronous motors are composed of phase-band harmonics, stator harmonics and rotor harmonics [11], where the harmonic order and angular frequency of the phase-band harmonics are shown in formula 1.

$$v = (6k_1 + 1)p_i \quad \omega_1. \tag{1}$$

The harmonic order and angular frequency of stator teeth are shown in formula 2.

$$v_t = k_1 Z_1 + p_i \quad \omega_1. \tag{2}$$

The harmonic order and angular frequency of the rotor teeth are shown in formula 3.

$$u_t = k_2 Z_2 + p_i \left[ 1 + k_2 \frac{Z_2}{p_i} (1 - s) \right] \omega_1. \tag{3}$$

Among them,  $k_1 = \pm 1, \pm 2, \dots$ ,  $k_2 = \pm 1, \pm 2, \dots$ ,  $Z_1$  is the number of stator slots,  $Z_2$  is the number of rotor slots,  $\omega_1$  is the angular frequency of the fundamental magnetic field,  $s$  is the slip and  $p_i$  is the number of pole pairs.

The radial electromagnetic density of the motor is a traveling wave that changes with time and space. After a series of harmonics of the same order and frequency are synthesized by a vector, the air gap flux density is shown in formula 4 [18].

$$\begin{aligned}
 b_r(\theta, t) = & b_p + \sum_v b_v \\
 & + \sum_\mu b_\mu = B_p \cos(p\theta - \omega_1 t - \varphi_m) \\
 & + \sum_v B_v \cos(v\theta - \omega_1 t - \varphi_v) \\
 & + \sum_\mu B_\mu \cos(\mu\theta - \omega_1 t - \varphi_\mu).
 \end{aligned} \tag{4}$$

Among them,  $b_p$  is the fundamental wave flux density,  $b_v$  is the stator tooth harmonic flux density, and  $b_\mu$  is the rotor

tooth harmonic flux density,  $B_p$  is the amplitude of the fundamental wave,  $B_v$  is the harmonic amplitude of the stator teeth,  $B_\mu$  is the rotor tooth harmonic amplitude,  $v$  is the order of stator harmonic,  $\mu$  is the order of rotor harmonic,  $\varphi_m$  is the initial phase of the fundamental wave,  $\varphi_v$  is the initial phase of stator tooth harmonic and  $\varphi_\mu$  is the initial phase of rotor tooth harmonic.

The fundamental frequency of the magnetic field force wave is twice as big as the frequency of the power supply and the frequency of the harmonics are shown in formula 6.

$$f = 2f_1 = 100\text{Hz}. \tag{5}$$

$$\begin{aligned}
 r = v_t - \mu_t, \quad f &= \left| k_2 \frac{Z_2}{p} (1 - s) \right| f_1, \\
 r = v_t + \mu_t, \quad f &= \left| k_2 \frac{Z_2}{p} (1 - s) + 2 \right| f_1,
 \end{aligned} \tag{6}$$

where  $r$  is the order of the force wave under the stator-rotor harmonic interaction which includes two forms:  $v_t - \mu_t$  and  $v_t + \mu_t$ ,  $v_t$  is the order of stator harmonic, and  $\mu_t$  is the order of rotor harmonic.

According to MAXWELL tensile stress theory, the radial electromagnetic force is shown in formula 7.

$$p_r(\theta, t) = \frac{b_r^2(\theta, t)}{2\mu_0}, \tag{7}$$

where  $\mu_0$  is the vacuum permeability, which value is  $4\pi \times 10^{-7}$ .

Using formula 7 to calculate the radial electromagnetic force along the circumference formed by the inner wall of the stator under normal operation, eccentric operation and broken rotor bars operation when the motor is fully loaded, which are shown in Fig. 1.

The radial electromagnetic force density along the inner wall of the stator is shown in Fig. 1. The abscissa of Fig. 1 is the arc length of the circle formed by counterclockwise rotation with the intersection of the  $x$ -axis in Fig. 2 and the inner wall of the stator as the starting point. The circumference of the inner wall of the stator is 465 mm. It can be seen from Fig. 1a that when the motor is running normally, the radial electromagnetic force density along the circumference of the inner wall of the stator is strictly periodic. The motor is symmetrical and contains four electrodes. The electromagnetic force density on the inner wall of the stator at the electrodes is 0, so four sections of the same electromagnetic force density distribution curve are formed. When the motor is eccentric or the rotor bar is broken, the radial electromagnetic

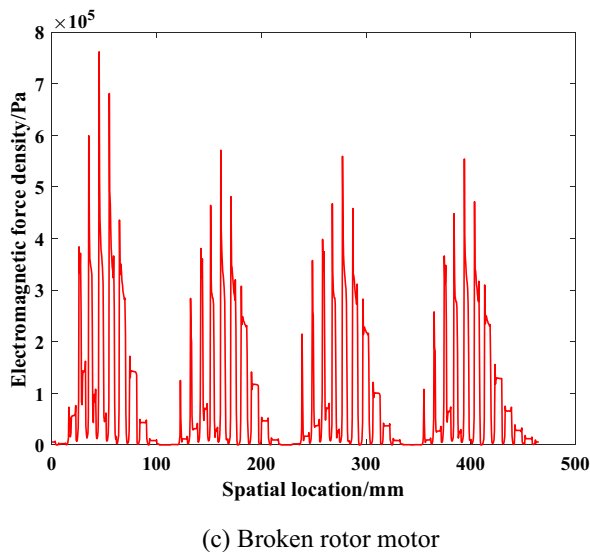
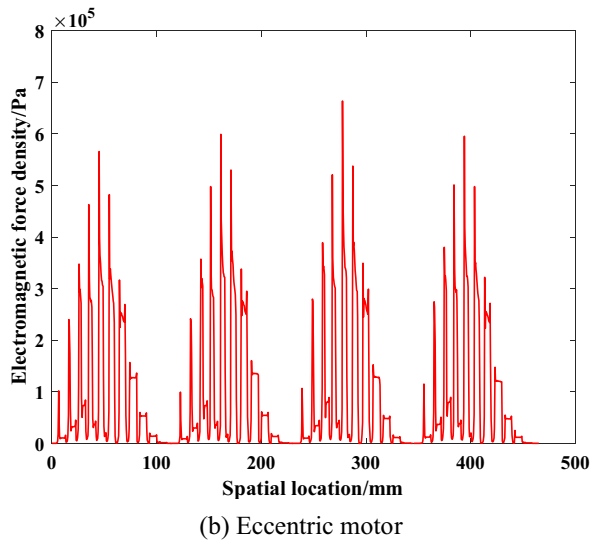
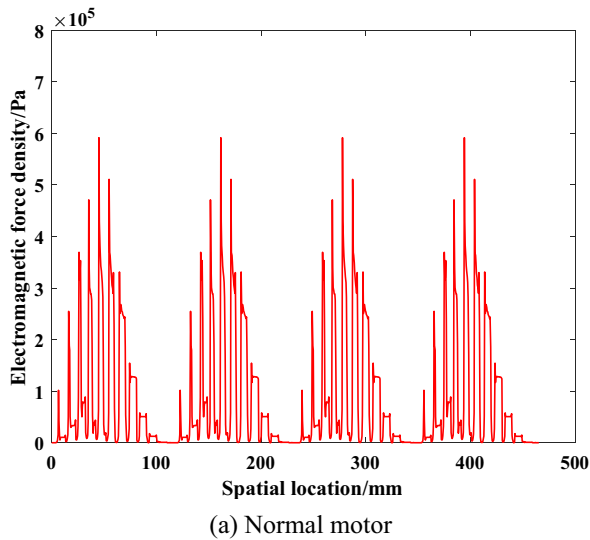


Fig. 1 Radial electromagnetic force density on the inner wall of the motor stator

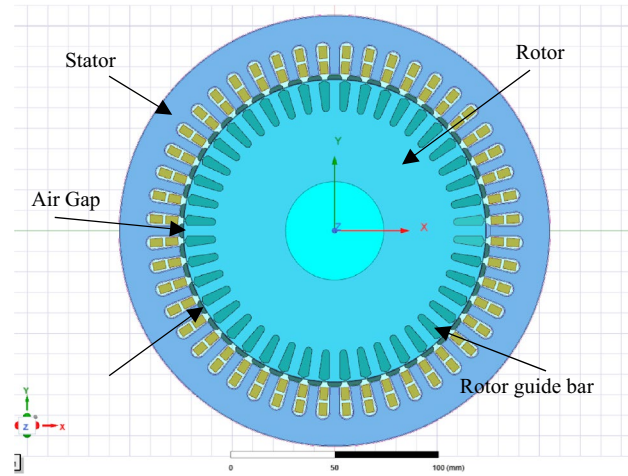


Fig. 2 Motor simulation model

force density on the inner wall of the stator has change. The motor eccentricity is shown in Fig. 1b. When the motor is eccentric, the radial electromagnetic force density varies slightly on the entire circumference, which is caused by the uneven distribution of air gaps after eccentricity. Where the air gap of the motor is small, the leakage flux is small, the magnetic field loss is small, and the radial electromagnetic force density is large, and the opposite is true in the place where the air gap is large. The broken bar of the motor will generate an additional magnetic field, resulting in a significant increase in the radial electromagnetic force density in the first 1/4 of the circumference.

### Calculation of Motor Vibration Acceleration Based on Frequency Response

The response of the structure is equal to the excitation multiplied by the frequency response function. If the frequency response function has a peak at the excitation frequency, the structure will vibrate severely. The frequency response technology is usually used to analyze the vibration response results of the structure after being excited by the excitation source. Frequency response is a technology to determine the steady-state response of the system when the structure is subjected to one or more harmonic loads.

Usually, the motion control formula is shown in formula 8 [19].

$$[M]\{\ddot{X}\} + [B]\{\dot{X}\} + [K]\{X\} = \{F\}\sin(\theta t). \tag{8}$$

Among them,  $[M]$  is the mass matrix,  $[B]$  is the damping matrix,  $[K]$  is the stiffness matrix,  $\{F\}\sin(\theta t)$  is the nodal

force vector,  $\{\ddot{X}\}$  is the nodal acceleration vector,  $\{\dot{X}\}$  is the nodal velocity vector, and  $\{X\}$  is the nodal displacement vector.

The displacement response of the core node is shown in formula 9.

$$\{X\} = \{A\}\sin(\theta t + \varphi). \tag{9}$$

Substitute formula 9 into formula 8 to get formula 10.

$$\{A\} = [-M\theta^2\sin(\theta t + \varphi) + K\sin(\theta t + \varphi) + B\theta\cos(\theta t + \varphi)]^{-1} \{F\}\sin(\theta t). \tag{10}$$

Among them,  $A$  is the amplitude vector and  $\varphi$  is the phase angle.

Formula 10 is solved by the finite element analysis (FEA) method, the frequency range and interval of  $\theta$  are set, and the displacement value is calculated, and the relationship between acceleration and force wave frequency can be obtained.

FEA uses a mathematical approximation to simulate real physical systems, which decomposes the entire problem area when solving, and each sub-area becomes a simple part, which is called an element. FEA can solve the relationship between element nodal force and nodal displacement, velocity and acceleration according to the material, shape, size, node number, position and other properties of the element.

### Analysis of Motor Frequency Response Under Electromagnetic Excitation

This article uses a general-purpose three-phase induction motor, which model is YZD132-4, the motor parameters are shown in Table 1.

The motor simulation model is shown in Fig. 2.

After the three-phase symmetrical current is applied, the air-gap composite magnetic field is generated due to the interaction of the magnetic fields of the stator and the rotor, which generates a radial electromagnetic force wave acting on the inner wall of the stator. The radial electromagnetic

**Table 1** Parameters of three-phase induction motor

$P$	Number of pole pairs	2
$N_S/N_R$	Number of stator/rotor slots	48/44
$M$	Number of phase	3
$n_N$	Synchronous speed	1500 r/min
$n$	Rated speed	1440 r/min
$f_1$	Working frequency	50 Hz
$\delta$	Air gap size	0.35 mm

force wave formed by the interaction between the radial component of the stator air gap magnetic field and the radial component of the rotor air gap magnetic field is the main factor causing the electromagnetic vibration of the motor.

When most motors work normally, the load rate is generally equal to or close to the rated load. Under the rated load, the vibration of the motor is relatively large, and the impact on the health of the motor is also relatively large. In addition, when the load of the motor increases, to improve the output capacity, the speed of the motor will decrease, so that the slip ratio of the motor will increase. The frequency of the electromagnetic excitation force generated by the interaction of the stator cogging harmonics and the rotor cogging harmonics changes after the slip ratio increases. If the frequency of the changed electromagnetic excitation force is closer to the natural frequency of the motor, the vibration of the motor will increase. Therefore, this paper takes the rated load as a typical working condition for analysis, and the motor is set to be in a rated load state and the rated speed is 1440 r/min.

When the motor is running, the eccentricity is allowed to be below 10%, and a slight broken rotor (one or two guide bars are broken) will not have a major impact on the short-term operation of the motor. This article considers the critical state in two cases, so the motor eccentric model is set with an eccentricity of 10%, and the motor broken bar model is set with two broken rotor bars. Considering that the motor's heat dissipation ribs and junction box have little effect on the vibration of the motor, to reduce the amount of calculation and facilitate the setting of sampling points, the motor structure model is simplified. The structure model does not consider the heat dissipation ribs and junction box.

The electromagnetic force at a certain point on the inner wall of the motor stator is shown in Fig. 3.

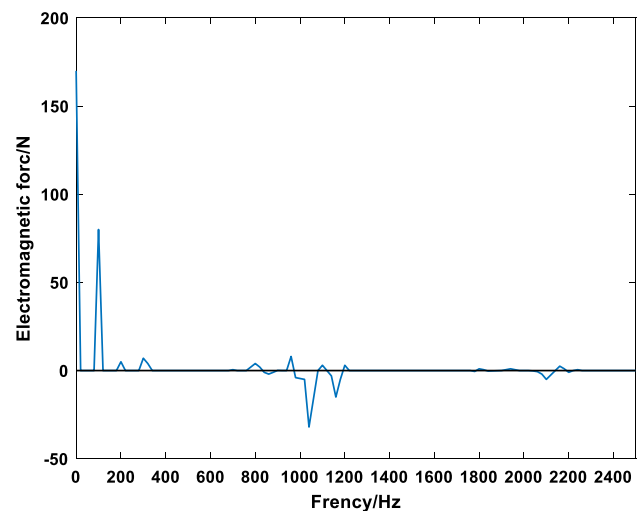


**Fig. 3** Electromagnetic force at a point on the inner wall of the stator

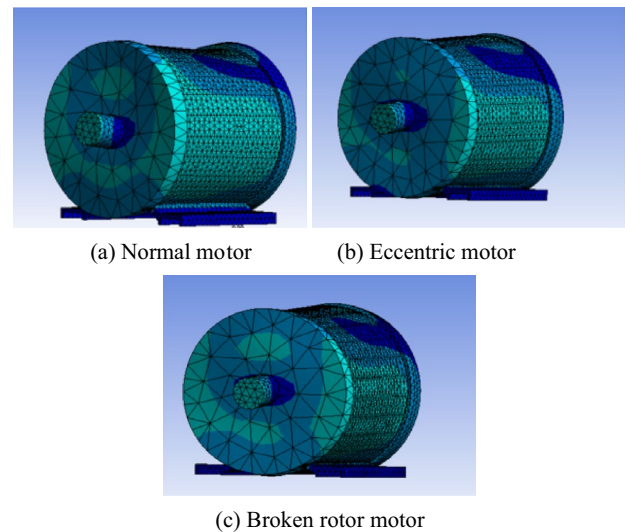
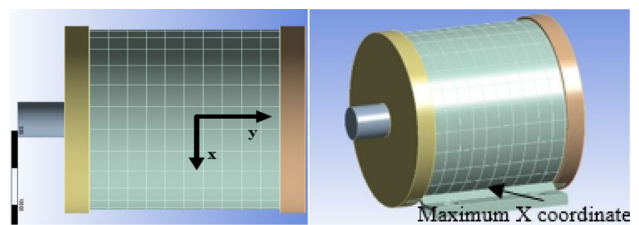
**Table 2** Main harmonic components of the motor

Main harmonic	Harmonic name	Theoretical value (Hz)	Simulation value (Hz)
$2f_1$	Double frequency	100	100
$N_R n_N$	First-order rotor slot harmonics	1056	1050
$N_R n_N - 2f_1$	First-order rotor slot harmonics	956	950
$N_R n_N + 2f_1$	First-order rotor slot harmonics	1156	1150
$N_S n_N$	First-order stator slot harmonics	1152	1150
$2N_R n_N$	Second-order rotor slot harmonics	2112	2100
$2N_R n_N - 2f_1$	Second-order rotor slot harmonics	2002	2000
$2N_R n_N + 2f_1$	Second-order rotor slot harmonics	2212	2200

The electromagnetic force fundamental wave frequency and harmonic frequency are obtained by simulation calculation, and the theoretical value of electromagnetic force harmonics calculated by formulas 5 and 6. Comparing the simulation value with the theoretical value, as shown in Table 2. It can be known from Table 2 that the theoretical main harmonic components are consistent with those obtained by the simulation calculation. The reason for the error is the resolution of the ANSYS software when calculating the electromagnetic force.

In addition to the fundamental wave, the electromagnetic force of the motor also contains high-order harmonic components. The vibration of the induction motor is mainly caused by the first harmonic and the second harmonic [20]. The frequency range is shown in Table 2. Therefore, the electromagnetic force is set to a frequency range of 0–2500 Hz, and the solution interval is taken as 100. The motor base is set with a fixed constraint, which is equivalent to the motor base being fixed by screws. After the constraint conditions are set, the model is solved.

Electromagnetic force acts on the inner wall of the stator, so the deformation of the inner wall of the stator is the most serious. After being transmitted to the shell, the characteristics of vibration deformation are not obvious, and the vibration measurement point positions of the motor in different states cannot be accurately found, as shown in Fig. 4. Therefore, the motor shell is gridded and divided into  $20 \times 10$  rectangular grids, and each grid is equivalent to a measuring point. The maximum value of the vibration acceleration at each measuring point in the specified frequency range is Calculated, which display as a three-dimensional image. The origin of the coordinates is the center point of the top of the motor, the  $x$ -axis and  $y$ -axis directions are shown in Fig. 5, and the  $z$ -axis is the vibration acceleration amplitude in the specified frequency range. Each measuring point is regarded as a coordinate with a unit of 1, the  $x$ -axis coordinate range is  $-10$  to  $10$ ,

**Fig. 4** Motor vibration and deformation under different operating conditions**Fig. 5** Motor three-dimensional vibration coordinate system direction

and the  $y$ -axis coordinate range is  $-5$  to  $5$ . In reality, the distance between the bottom of the motor and the floor is very small, and the vibration sensor is difficult to install at the bottom of the motor, so the  $x$ -axis only reaches the base of the motor.

During eccentric operation and broken bar operation, the vibration on the motor casing is mainly caused by the radial electromagnetic force at the air gap. The radial electromagnetic force passes through the center of the motor section and is perpendicular to the motor axis, which can be decomposed into two directions:  $X$  (horizontal) and  $Y$

(vertical upward). Therefore, the vibration of the motor casing mainly includes the  $X$  direction and the  $Y$  direction, and the vibration in the  $Z$  (axial) direction is mostly caused by the vibration of the shaft system, which can basically be ignored in the electromagnetic vibration of the motor casing caused by the electromagnetic excitation

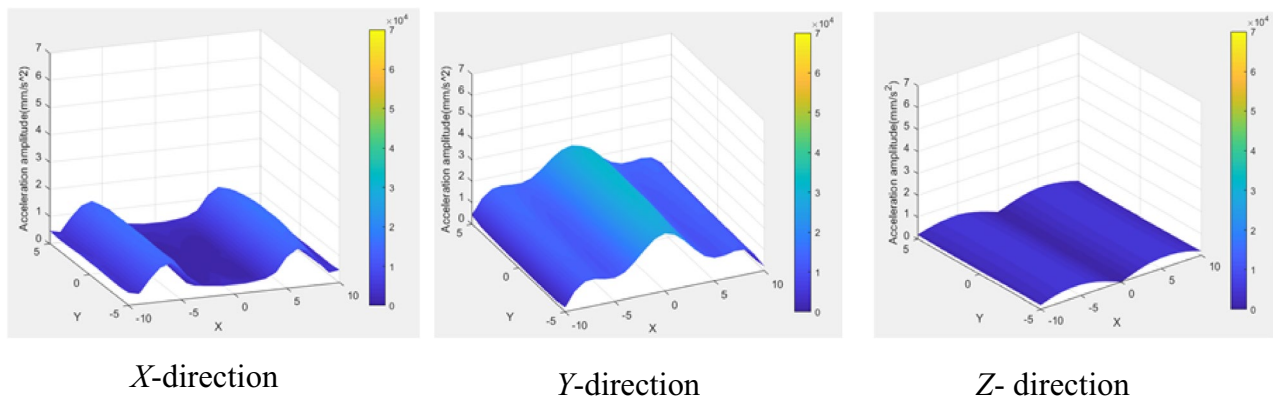


Fig. 6 Normal motor

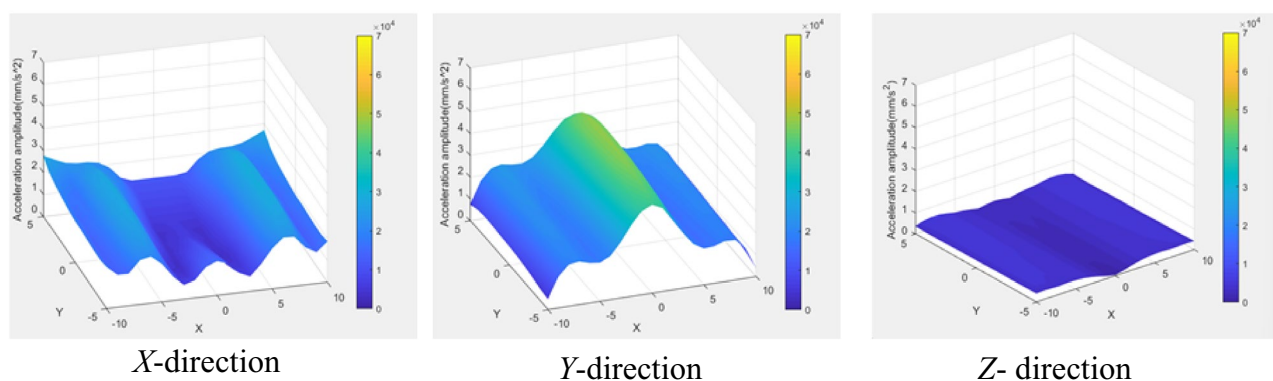


Fig. 7 Eccentric motor

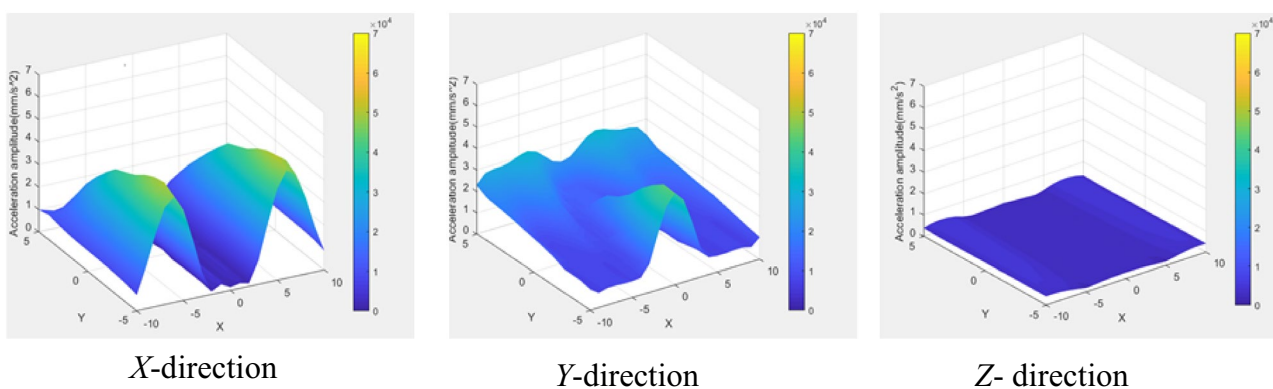


Fig. 8 Broken rotor motor

force. Therefore, the vibration acceleration signals in the  $X$  (horizontal) direction and  $Y$  (vertical upward) direction of the motor in normal operation, eccentric operation and broken bar operation are calculated, and the three-dimensional surface graphs are produced. The results are shown in Figs. 6, 7 and 8. In Figs. 6, 7 and 8, the  $z$ -axis is the amplitude of vibration acceleration, and the  $x$ -axis and  $y$ -axis are the coordinates of the measuring points for the division of the motor casing. The vibration amplitude of  $Z$ -direction is much smaller than that of  $X$ -direction and  $Y$ -direction, and the vibration characteristics of the motor under normal operation, eccentric operation and broken bar operation are difficult to distinguish, so this paper does not consider the vibration of  $Z$  direction.

It can be seen from Figs. 6, 7 and 8 that when the motor is running normally, the  $X$ -direction vibration is mainly concentrated on both sides of the motor, corresponding to the  $x$ -coordinates of 6 and  $-6$ , and the  $Y$ -direction vibration is mainly concentrated on the top of the motor, and the corresponding  $x$ -coordinate is 0. The vibration characteristics of the motor under eccentric operation are similar to those under normal operation. When the rotor of the motor is broken, both  $X$ -direction vibration and  $Y$ -direction vibration are concentrated at the front end of the motor, but the corresponding  $x$ -coordinate remains unchanged. Two vibration sensors are placed on the front and rear ends of the horizontal single side of the motor or two vibration sensors are placed on the front and rear of the top of the motor. Comparing the magnitude of the acceleration signals collected by the two vibration sensors can effectively distinguish whether the motor is broken. If the vibration sensors are installed on the horizontal side of the motor, and the

$X$ -direction vibration acceleration measured at the front end is much greater than the  $X$ -direction vibration acceleration measured at the rear end, the motor has a high probability of broken rotor bar failure. It can be seen from Figs. 6 and 8 that when the motor rotor is broken, the vibration characteristics in the  $X$ -direction are more significant than in the  $Y$ -direction. When only two vibration sensors are installed in consideration of the cost, the horizontal single-sided installation of the motor is preferred.

To distinguish between normal operation and eccentric operation of the motor, the motor base constraint is adjusted to find the vibration characteristics of the motor when the motor base screws have loose, which include the loosening of the left front screw of the motor base, the loosening of the left screws of the motor base, the loosening of the rear screws of the motor base and the loosening of the diagonal screws of the motor base. Figures 9, 10, 11 and 12 are shown that the base screws are loose when the motor is running normally, and Figs. 13, 14, and 16 are shown that the base screws are loose when the motor is eccentrically running.

It can be seen from Figs. 9, 10, 11, 12, 13, 14, 15 and 16 that if the screw on the front left of the base is loose and the screws on the left side of the base are loose, the vibration characteristics of the motor in normal operation and eccentric operation remain similar, which cannot be effectively distinguished. When the screws on the rear of the motor base are loose and the diagonal screws of the base are loose, there is a clear difference between the vibration characteristics of the motor in normal operation and eccentric operation. The difference in vibration characteristics is the most obvious when the screws on the rear of the base are loosened.

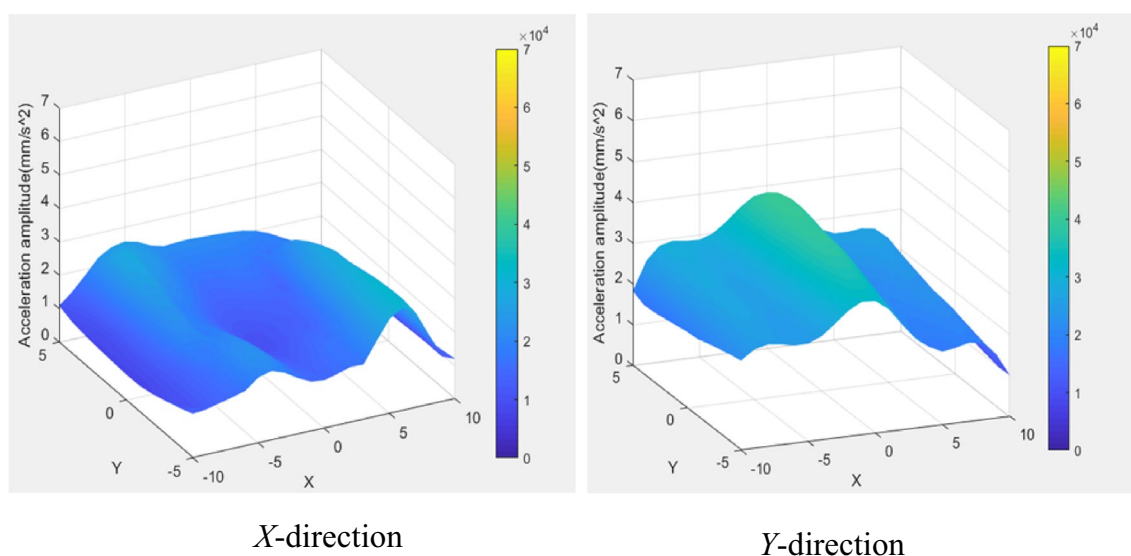
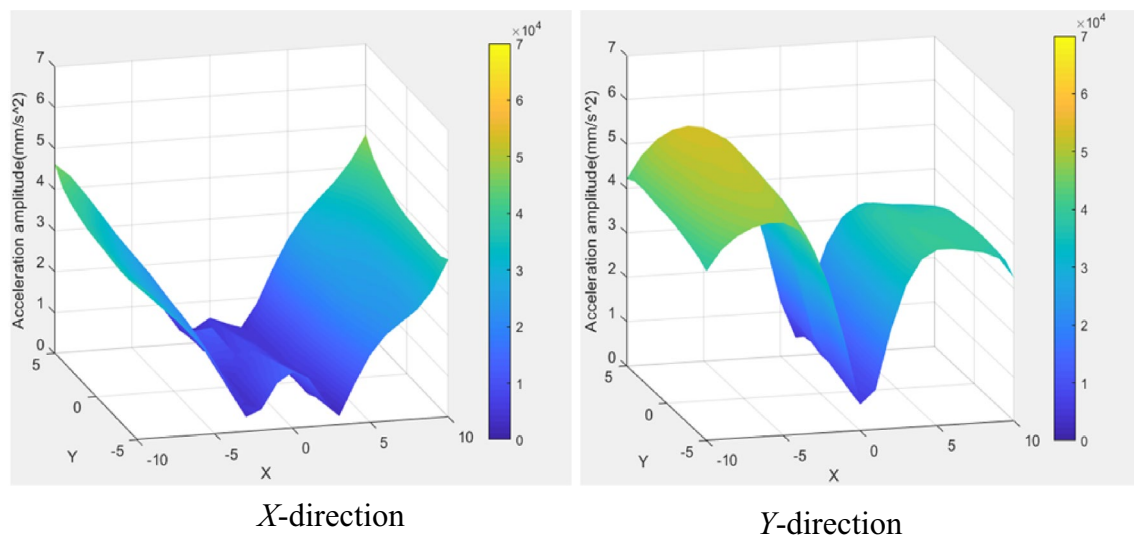
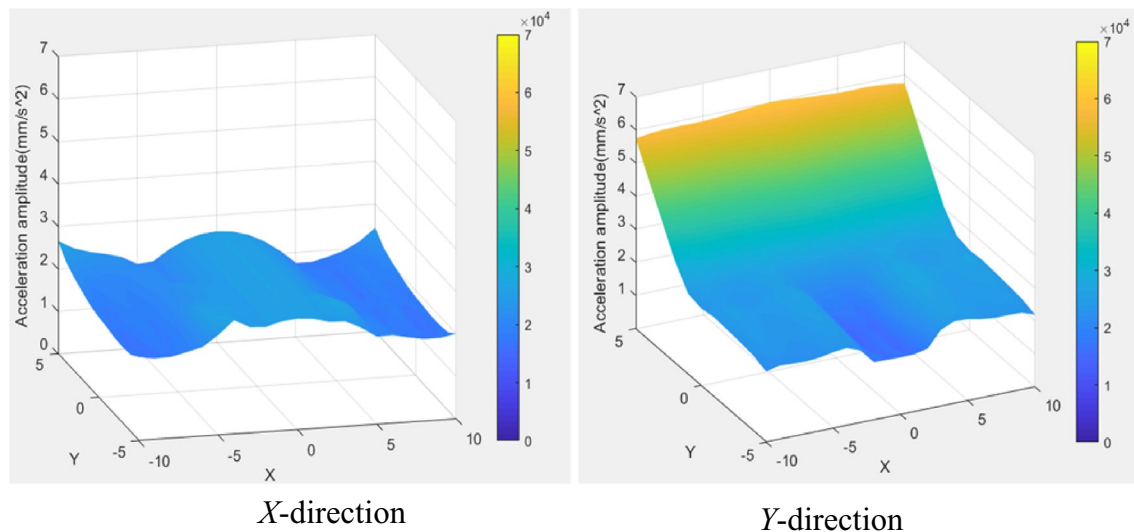


Fig. 9 Normal motor with the loosening of left front screw of the base





**Fig. 10** Normal motor with the loosening of left screws of the



**Fig. 11** Normal motor with the loosening of rear screws of the base

When the screws on the rear side of the motor base are loose, the vibration acceleration of each measuring point in the  $X$ -direction is roughly equal, while the vibration acceleration in the  $X$ -direction during eccentric operation is the largest at the front end adjacent to the top of the motor, and the corresponding  $x$ -coordinate is  $-3$  to  $3$ . When the motor runs normally and the diagonal screws of the base are loose, the vibration acceleration in the  $X$ -direction of the casing is the largest near the base. When the motor runs eccentrically and the diagonal screws of the base are loose, the vibration acceleration in the  $X$ -direction of the shell is similar

to that when the rear screws are loose. This proves that the loosening of the screws on the rear side of the motor base and the loosening of the diagonal screws of the motor base can increase the vibration characteristics of the motor when the motor is eccentric. In response to this phenomenon, two vibration sensors are placed at the front and rear of the top of the motor. By actively loosening the screws on the rear of the motor, if the  $X$ -direction vibration acceleration signals collected by the two sensors are approximately equal, the motor is in a normal state. If the  $X$ -direction vibration acceleration

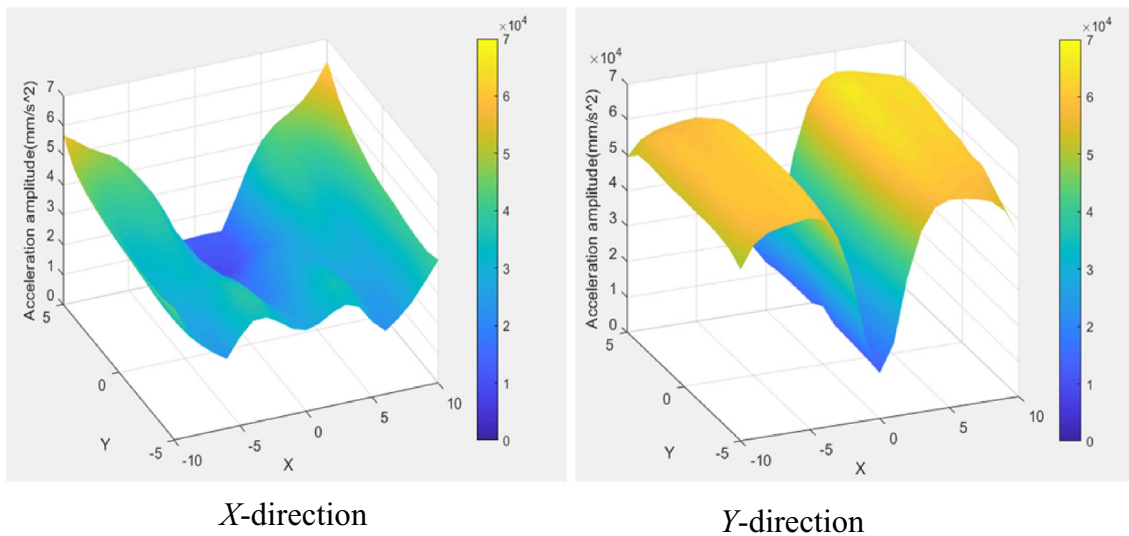


**Fig. 12** Normal motor with the loosening of diagonal screws of the base

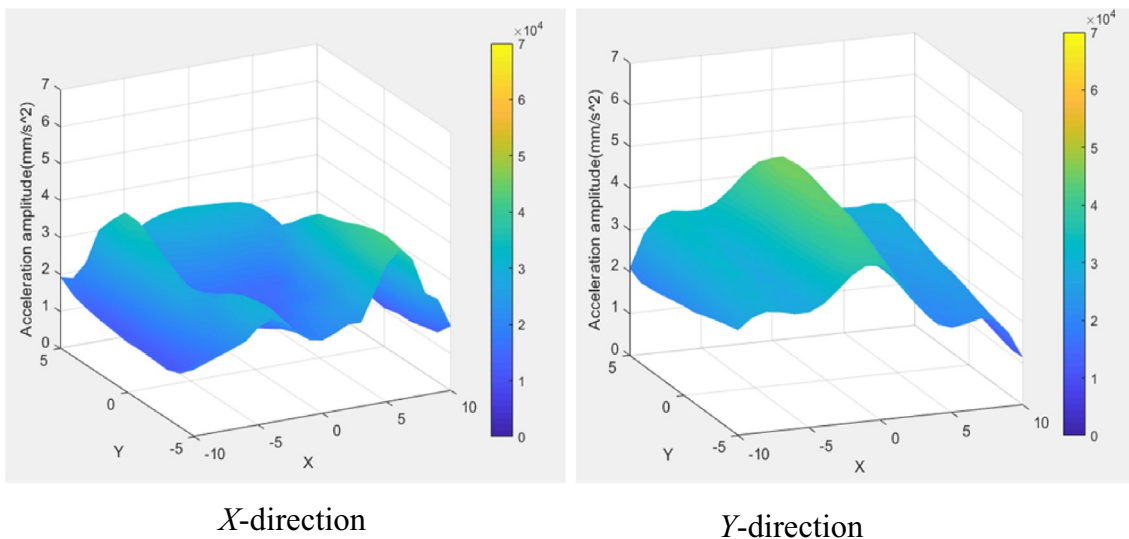


**Fig. 13** Eccentric motor with the loosening of left front screw of the base

in the front-end is much greater than the rear-end, the motor has a high probability of eccentricity.

The installation plan of the vibration sensor is obtained by combining the above analysis and the three-dimensional characteristic diagrams of vibration. A total of 7 vibration sensors are required. The installation positions are the front and rear of the top of the motor, the front and rear of the horizontal sides of the motor, and any position of the motor shell close to the base. For the convenience of description, the vibration acceleration signals measured by the 7 vibration sensors are given a definition number, which as

shown in Table 3, and the position of the vibration sensors in Table 3 are shown in Fig. 17.

In the actual operation of the motor, based on the vibration acceleration signals collected by the above seven sensors, the fault identification can be achieved.

1. When the motor is running normally, the vibration acceleration in the X-direction collected by the 7 sensors has  $X_3 \approx X_4 \approx X_5 \approx X_6 > X_1 \approx X_2 \approx X_7$ . The vibration acceleration in the Y-direction collected by the 7 sensors has  $Y_1 \approx Y_2 > Y_3 \approx Y_4 \approx Y_5 \approx Y_6 > Y_7$ .

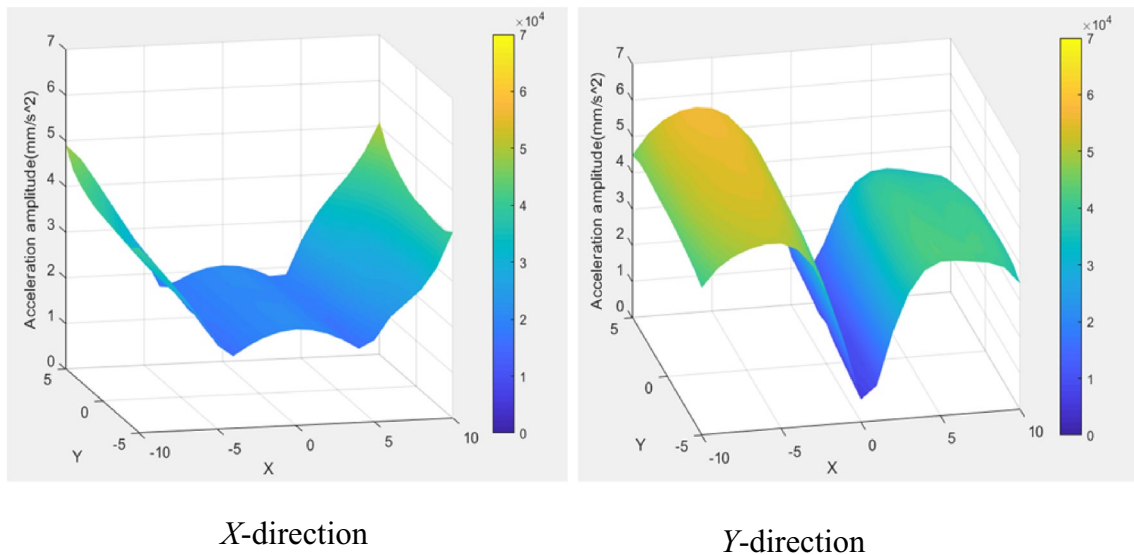


Fig. 14 Eccentric motor with the loosening of left screws of the base

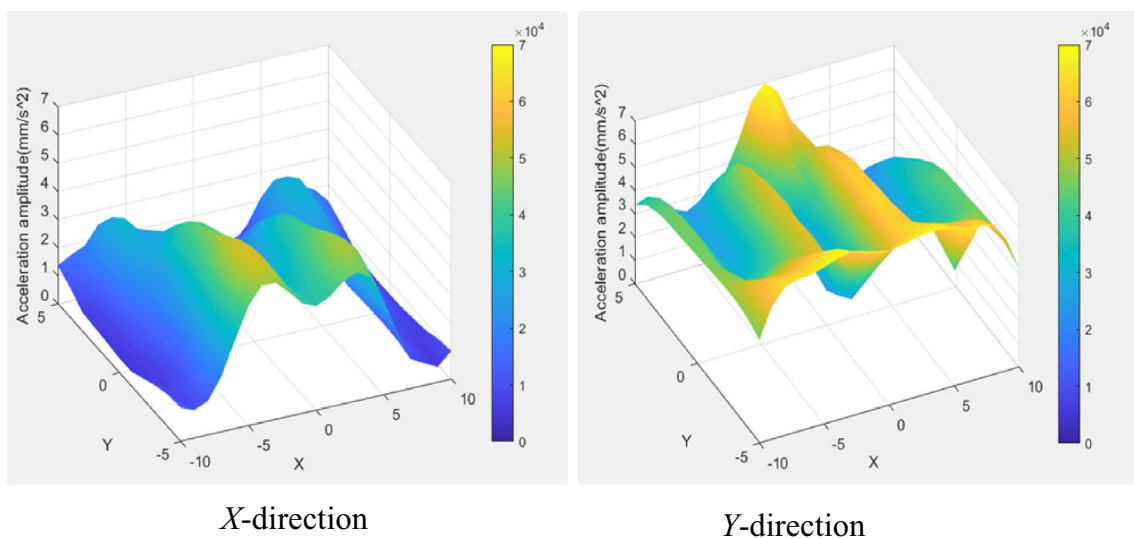


Fig. 15 Eccentric motor with the loosening of rear screws of the base

2. When the motor is running with broken bars, the vibration acceleration in the *X*-direction collected by the 7 sensors has  $X_3 \approx X_5 > X_4 \approx X_6 \approx X_7 > X_1 \approx X_2$ . The vibration acceleration in the *Y*-direction collected by the 7 sensors has  $Y_1 > Y_4 \approx Y_6 > Y_2 > Y_7 > Y_3 \approx Y_5$ .
3. The vibration characteristics of the motor during eccentric operation are similar to those during normal operation. By loosening the screws on the rear of the

- motor base, if  $X_1 \approx X_2 > X_3 \approx X_4 \approx X_5 \approx X_6 > X_7$ , the motor is in normal operation. If  $X_1 > X_3 \approx X_5 > X_4 \approx X_6 > X_2 \approx X_7$ , the motor has a high probability of eccentric fault.
4. According to the symmetry of the motor, the other kinds of base screw looseness that have not been simulated can be obtained, which is shown in Table 4.

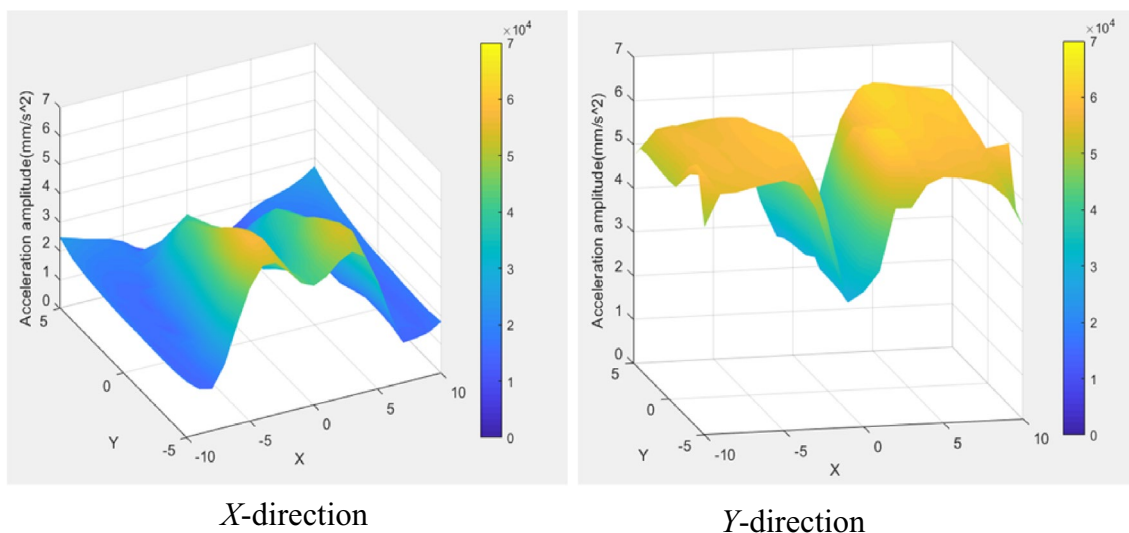


Fig. 16 Eccentric motor with the loosening of diagonal screws of the base

Table 3 Vibration acceleration sensor number

Sensor number	Vibration acceleration	Installation coordinates	Definition
1	$X_1$	(0, -5)	X-direction vibration acceleration at the front end of the motor top
	$Y_1$	(0, -5)	Y-direction vibration acceleration at the front end of the motor top
2	$X_2$	(0, 5)	X-direction vibration acceleration at the rear end of the motor top
	$Y_2$	(0, 5)	Y-direction vibration acceleration at the rear end of the motor top
3	$X_3$	(-6, -5)	X-direction vibration acceleration at the left front end of the motor horizontally
	$Y_3$	(-6, -5)	Y-direction vibration acceleration at the left front end of the motor horizontally
4	$X_4$	(-6, 5)	X-direction vibration acceleration at the left rear end of the motor horizontally
	$Y_4$	(-6, 5)	Y-direction vibration acceleration at the left rear end of the motor horizontally
5	$X_5$	(6, -5)	X-direction vibration acceleration at the right front end of the motor horizontally
	$Y_5$	(6, -5)	Y-direction vibration acceleration at the right left front end of the motor horizontally
6	$X_6$	(6, 5)	X-direction vibration acceleration at the right rear end of the motor horizontally
	$Y_6$	(6, 5)	Y-direction vibration acceleration at the right rear end of the motor horizontally
7	$X_7$	(10, 0)	X-direction vibration acceleration of the motor near the base
	$Y_7$	(10, 0)	Y-direction vibration acceleration of the motor near the base

The installation of 7 vibration sensors can meet different test requirements. Different numbers of sensors can be configured according to actual needs. Two vibration sensors, sensor 3 and sensor 4, can be installed when the motor has broken bars. If  $X_3 \gg X_4$ , the motor has a high probability of broken bars. Two vibration sensors, sensor 1 and sensor 2, can be installed when the motor has an eccentric fault. By loosening the screws on the rear side

of the motor base, if  $X_1 \gg X_2$ , the motor has a high probability of eccentricity failure.

To sum up, seven triaxial acceleration sensors and multi-channel data acquisition cards are required to monitor the operating states of all the motors studied in this paper, and the total cost is between \$1700 and \$3500. For some important and expensive motors, such as mine motors for vibration monitoring, the cost of this method is not high. The method in this paper can also judge the running state of the motor only by monitoring the X-axis vibration acceleration or the

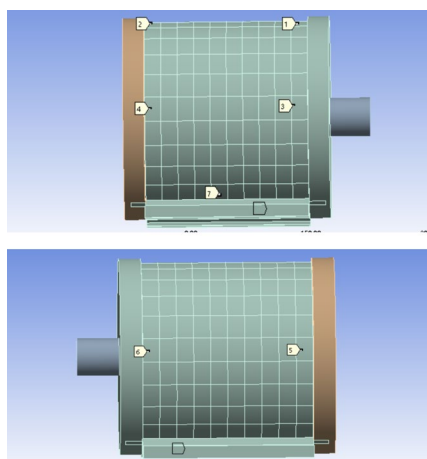


**Fig. 17** The location layout of the vibration sensors

Y-axis vibration acceleration. For motors with low monitoring efficiency requirements, a single-axis acceleration sensor can be used instead of a three-axis acceleration sensor, thereby greatly saving costs. In addition, according to the research in this paper, the number and installation locations of vibration sensors can be adjusted according to the type of fault that needs to be monitored.

The method proposed in this paper is to be used for online monitoring of motor vibration, and real-time comparison is made according to the vibration signals collected by each sensor to analyze the running state of the motor. The sensorless vibration harmonic estimation method proposed in citation [11] needs to collect the current and position signals in the motor for multi-step calculation to estimate the motor vibration signal, which requires more time to estimate and calculation than the traditional vibration sensor to collect the vibration signal, and this method estimates the vibration frequency of

**Table 4** Comparison of vibration acceleration when the motor base screws are loose

A single screw on the motor base is loose	The left front screw of the base is loose	$X_4 \approx X_5 > X_3 \approx X_6 > X_1$ $\approx X_2 \approx X_7$ $Y_1 \approx Y_2 > Y_3 \approx Y_4 > Y_5$ $\approx Y_6 > Y_7$
	The rear left screw of the base is loose	$X_3 \approx X_6 > X_4 \approx X_5 > X_1$ $\approx X_2 \approx X_7$ $Y_1 \approx Y_2 > Y_3 \approx Y_4 > Y_5$ $\approx Y_6 > Y_7$
	The right front screw of the base is loose	$X_3 \approx X_6 > X_4 \approx X_5 > X_1$ $\approx X_2 \approx X_7$ $Y_3 \approx Y_4 > Y_1 \approx Y_2 > Y_5$ $\approx Y_6 > Y_7$
	The right rear screw of the base is loose	$X_4 \approx X_5 > X_3 \approx X_6 > X_1$ $\approx X_2 \approx X_7$ $Y_3 \approx Y_4 > Y_1 \approx Y_2 > Y_5$ $\approx Y_6 > Y_7$
The screws on the horizontal side of the base are loose	The left screws of the base are loose	$X_7 > X_5 \approx X_6 \approx X_3 \approx X_4$ $> X_1 \approx X_2$ $Y_3 \approx Y_4 > Y_7 > Y_5 \approx Y_6$ $> Y_1 \approx Y_2$
	The right screws of the base are loose	$X_7 > X_5 \approx X_6 \approx X_3 \approx X_4$ $> X_1 \approx X_2$ $Y_5 \approx Y_6 > Y_3 \approx Y_4 > Y_7$ $> Y_1 \approx Y_2$
The screws on the front or rear side of the base are loose	The rear screws of the base are loose	$X_1 \approx X_2 > X_3 \approx X_4 \approx X_5$ $\approx X_6 > X_7$ $Y_2 \approx Y_4 \approx Y_6 > Y_7 > Y_1$ $\approx Y_3 \approx Y_5$
	The front screws of the base are loose	$X_1 \approx X_2 > X_3 \approx X_4 \approx X_5$ $\approx X_6 > X_7$ $Y_5 \approx Y_6 > Y_3 \approx Y_4 > Y_7$ $> Y_1 \approx Y_2$
The diagonal screws of the base are loose	The diagonal screws of the base are loose	$X_7 > X_3 \approx X_4 \approx X_5 \approx X_6$ $> X_1 > X_2$ $Y_3 \approx Y_4 \approx Y_5 \approx Y_6 > Y_7$ $> Y_1 \approx Y_2$

**Table 5** Comparison of this method with other methods

Method	Cost	Calculation speed	Considered motor operating conditions
Method of this paper	Between \$1700 and \$3500	Fast	Multiple conditions
Sensorless method	\$1000+	Very slow	Single condition
Non-contact vibration measurement system	\$4000+	Slow	Single condition

3.8 Hz in about 1 s, which will undoubtedly use more time for high-frequency vibrations. The method in this paper compares the real-time vibration signals collected by each sensor to determine the running state of the motor, which will undoubtedly greatly reduce the diagnosis time. The comparison between this method and other methods is shown in Table 5.

## Conclusion

Vibration signal is an important indicator for condition monitoring and diagnosis of induction motor. When the installation position of the vibration sensors is not suitable, the obtained vibration signal will not accurately reflect the vibration characteristics of the motor. Aiming at this problem, this paper proposes a vibration sensor layout optimization method based on the frequency response of motor vibration. The method obtains an optimal layout scheme of multiple vibration sensors by analyzing the three-dimensional vibration characteristic surface map of the motor under the action of the electromagnetic force, which can more accurately collect the vibration characteristic signal of the motor. Preliminary identification of motor faults can be achieved through different combinations of vibration sensors. The following conclusions are drawn from the research of this paper.

1. The vibration characteristics of the motor casing under different operating conditions are different. When the motor eccentricity is small, the impact on the motor vibration is small, and the vibration characteristics of the casing are similar to those in normal operation. The broken rotor bar of the motor has a great influence on the vibration of the motor, and the vibration characteristics of the casing are significantly different from those in normal operation. Compared with the literature that only considers a single operating condition, the method in this paper considers more comprehensively, and more suitable for on-site comprehensive monitoring of motor vibration health status.
2. The multi-sensor fusion analysis method can judge and distinguish different faults through the combined characteristics of different measuring point sensors. Using 7 sensors can meet various test requirements. In addition, two vibration sensors can be installed for motor eccentricity failure, and two vibration sensors can be installed for motor broken bar failure. There are many types of loose screws on the motor base, and 7 sensors are required for joint sampling. Compared with the methods in the citation that only consider the vibration sensor layout, the method proposed in this paper enables more comprehensive health and fault diagnosis.
3. After the motor base screws are loosened, the vibration characteristics of the casing will be merged with the original vibration characteristics under the current operating conditions, and the new characteristics after fusion will expand the original vibration characteristics of the motor. For the eccentric operation of the motor, the looseness of the screws on the rear side of the base and the looseness of the diagonal screws of the base can amplify the fault vibration characteristics and help identify the fault characteristics. Therefore, in the process of motor health diagnosis, the vibration characteristics of the motor casing can be obtained by actively loosening the screws, so as to determine whether the motor is eccentric.

Compared with the existing vibration sensor installation method, this method has strong versatility and can accurately collect vibration characteristics under a variety of operating conditions. Compared with the sensorless vibration signals estimation method, this method has higher acquisition accuracy and the calculation speed is fast. This method provides a reference for other equipment to set vibration sampling

points, and provides reliable data support for the state monitoring and fault diagnosis of the three-phase induction motor.

## Declarations

**Conflict of interest** On behalf of all authors, the corresponding author states that there is no conflict of interest.

## References

- Cai J, Chen X, Sihan Wu, Sui X (2019) Motor vibration signal acquisition and detection system based on STM32. *Sensors and Microsystems* 38(11):108–110
- Cruz-Vega I, Rangel-Magdaleno J, Ramirez-Cortes J et al (2017) Automatic progressive damage detection of rotor bar in induction motor using vibration analysis and multiple classifiers. *J Mech Sci Technol* 31:2651–2662. <https://doi.org/10.1007/s12206-017-0508-3>
- Morales-Perez C, Rangel-Magdaleno J, Peregrina-Barreto H, Amezquita-Sanchez JP, Valtierra-Rodriguez M (2018) Incipient broken rotor bar detection in induction motors using vibration signals and the orthogonal matching pursuit algorithm. *IEEE Trans Instrum Meas* 67(9):2058–2068. <https://doi.org/10.1109/TIM.2018.2813820>
- Mustafa EKER, Mehmet AKAR (2016) Eccentricity fault diagnosis in permanent magnet synchronous motors via vibration signal. *J Gaziosmanpasa Sci Res Issue* 13:87–102
- Panigrahy PS, Chattopadhyay P (2020) Tri-axial vibration based collective feature analysis for decent fault classification of VFD fed induction motor. *Measurement* 168:108460
- Xin H (2021) Sensor installation method and comparative analysis in vibration test. *China Inspect Test* 29(02):24–26+5
- Xunwen S, Shaoping W, Dongmei Z, Shi J (2011) Analysis of harmonic response of reducer in helicopter and optimal layout of sensors. *J Beijing Univ Aeronaut Astronaut* 37(09):1049–1053
- Tianling G, Weiqiu C (2017) Analysis and treatment of wind turbine generator tripping faults frequently triggered by over-vibration protection. *Guangdong Electric Power* 30(02):54–58
- Guilan W, Hongshan Z, Shuangwei G et al (2017) Numeric optimal sensor configuration solutions of wind turbine gearbox based on structure analysis. *IET Renew Power Gener* 11(12):1597–1602
- Azzedine B, Lias R, Zoubir Z, Mounir G (2016) The influence of the sensor position on the quality of the vibration measurement of rotating machinery on flexible supports. *Int Conf Syst Reliab Sci (ICSRS)* 2016:68–71. <https://doi.org/10.1109/ICSRS.2016.7815840>
- Huang C, Yang S (2020) Sensorless Vibration Harmonic Estimation of Servo System Based on the Disturbance Torque Observer. *IEEE Trans Industr Electron* 67(3):2122–2132. <https://doi.org/10.1109/TIE.2019.2907443>
- Dutta S, Basu B, Talukdar FA (2021) Classification of induction motor fault and imbalance based on vibration signal using single antenna's reactive near field. *IEEE Trans Instrum Meas* 70:1–9. <https://doi.org/10.1109/TIM.2021.3108230> (Art no. 3524209)
- Roy D, Sinharay A, Bhowmick B, Rakshit R, Chakravarty T, Pal A (2020) A novel RF-assisted-strobe system for unobtrusive vibration detection of machine parts. *IEEE Sens J* 20(18):10924–10935. <https://doi.org/10.1109/JSEN.2020.2995513>
- Zhang Z, Liu C, Li H et al (2017) Optical fiber grating vibration sensor for vibration monitoring of hydraulic pump. *Photonic Sens* 7:140–147. <https://doi.org/10.1007/s13320-017-0403-7>
- Li Q, Liu X, Zhao L et al (2017) A novel vibration sensor based on phase grating interferometry. *Appl Phys B* 123:162. <https://doi.org/10.1007/s00340-017-6724-9>
- Debnath B, Kumar R (2020) A new tapered-L shaped springs-based MEMS piezoelectric vibration energy harvester designed for small rolling bearing fault detection. *Microsyst Technol* 26:2407–2422. <https://doi.org/10.1007/s00542-020-04783-z>
- Du J, Li Y, Yu Z, Wang Z (2020) Characterization of radial electromagnetic force and vibration response in squirrel-cage induction motor under PWM supply. In: 2020 IEEE international conference on applied superconductivity and electromagnetic devices (ASEMD), p 1–2. <https://doi.org/10.1109/ASEMD49065.2020.9276162>
- Wei S, Mubayar E, Min L (2015) Calculation of induction motor electromagnetic force and its influence on motor vibration. *Motors Control Appl* 42(11):41–46
- Ling W, Changsheng Z, Jiajing F (2012) Analysis of electromagnetic vibration of induction motor based on finite element. *Vib Shock* 31(02):140–144+154
- Kong D, Shuai Z, Li W, Wang D (2019) Electromagnetic vibration characteristics analysis of a squirrel-cage induction motor under different loading conditions. *IEEE Access* 7:173240–173248. <https://doi.org/10.1109/ACCESS.2019.2956950>

**Publisher's Note** Springer Nature remains neutral with regard to jurisdictional claims in published maps and institutional affiliations.